Passive seismic full waveform inversion with unknown onsets in an orthorhombic anisotropic medium

Hanchen Wang & Tariq Alkhalifah, King Abdullah University of Science and Technology

SUMMARY

Full waveform inversion (FWI) based methods are getting more attractive in passive seismic (microseismic) monitoring studies. A high resolution knowledge of the medium in which the events occur is crucial to proper monitoring. In most cases, not only the velocity, but also the anisotropy has a large influence on locating passive events related to hydraulic fracturing. Due to the inherent anisotropy nature of most rocks associated with unconventional reservoirs, accounting for anisotropy is even more important in such investigations. We propose a 3D acoustic orthorhombic FWI method for passive seismic events to invert for the source image, source function and the model parameters, without any a prior knowledge about source location or source function in time. In order to mitigate the effect of the unknown source ignition time, we convolve reference traces with the observed and modeled data. A total variation regularization is applied to improve the robustness of the model parameters inversion considering the limited sources and illumination angles of microseismic experiments. The adjoint-state method is used to derive the gradient for the source image, source function and the anisotropic model parameters. The proposed method produces good estimates of the source location and the model structures for the modified orthorhombic 3D SEG/EAGE overthrust model.

INTRODUCTION

Hydraulic fracturing is one of the most commonly used and promising methods in unconventional reservoir exploration (Warpinski et al., 2009). The main goal of hydraulic trearments is to create high pressure conditions and enable easier exploitation by injecting water or other fluids in the target area (Van Der Baan et al., 2013). The injection process often ignites passive events, which can be monitored through sensors in a monitoring well or on the Earth's surface. Through the monitoring, the locations of the passive seismic events are usually estimated, which in turn can help us monitor the fracturing process. Such information helps the engineers estimate the stimulated rock volume (SRV) and optimize their injection strategy (Grechka and Yaskevich, 2013). Thus, it is critical to have a detailed understanding of how a formation is fractured through locating those passive events.

Many methods have been proposed to locate the passive seismic sources. Conventional methods based on traveltime (Eisner et al., 2009) and migration techniques (Nakata and Beroza, 2016; Wang and Alkhalifah, 2017) have their own advantages (low computational cost) and disadvantages (instability and inaccuracy), which is mainly due to the model misfit to the true earth. Recently, more advanced methods, for example FWI methods, allow us to estimate source locations with a crude guess of the model, because only an approximate starting model is needed since the inversion is also tasked with updating the model by a data matching objective (Kaderli et al., 2015; Sun et al., 2016; Wang and Alkhalifah, 2018). Most existing FWI methods for microseismic assume the earth to be isotropic and treat the problem in a 2D plane, which reduces the computational cost at the expense of simplifying the true Earth (3D and anisotropic) and introducing inaccuracies in locating passive events in complex regions.

In this abstract, a 3D orthorhombic anisotropic FWI method is proposed to update the spatial and the temporal information of the source and a convolution based FWI approach is used to update the anisootropic parameters of the model in order to better describe the anisotropy in the medium and in the mean time overcome the difficulty of the unknown passive source onset times. A synthetic test on a modified 3D orthorhombic SEG/EAGE overthrust model is given to show the effectiveness of the proposed method.

THEORY

The acoustic wave propagation in a 3D orthorhombic medium satisfies the following wave equation in the frequency domain (Alkhalifah, 2003):

$$-\omega^6 P - A\omega^4\frac{\partial^2 P}{\partial x^2} - B\omega^4\frac{\partial^2 P}{\partial y^2} - C\omega^4\frac{\partial^2 P}{\partial z^2} + D\omega^2\frac{\partial^4 P}{\partial x^2\partial y^2} + E\omega^2\frac{\partial^4 P}{\partial x^2\partial z^2} + F\omega^2\frac{\partial^4 P}{\partial y^2\partial z^2} - G\frac{\partial^6 P}{\partial x^2\partial y^2\partial z^2} = S(\omega) \tag{1}$$

where P is the pressure field in the frequency domain at location (x,y,z), $S(\omega)$ is the source term. The coefficients can be written in the forms of orthorhombic parameters (Ibanez-Jacome et al., 2014):

$$\begin{aligned} &A = v_{n1}^2(1+2\eta_1), B = v_{n2}^2(1+2\eta_2), C = v_v^2,\\ &D = v_{n1}^2(1+2\eta_1)[v_{n1}^2(1+2\eta_1)\chi^2 - v_{n2}^2(1+2\eta_2)],\\ &E = -2\eta_1 v_{n1}^2 v_v^2, F = -2\eta_2 v_{n2}^2 v_v^2,\\ &G = -v_v^2 v_{n1}^2[v_{n1}^2(1+2\eta_1)^2\chi^2 - 2\chi(1+2\eta_1)v_{n1}v_{n2} + v_{n2}^2(1-4\eta_1\eta_2)]. \end{aligned} \tag{2}$$

The acoustic approximation is useful when only single component or pressure recording is available, which is the case most of the time. The anisotropic parameters are defined in detail in Alkhalifah (2003) and Masmoudi and Alkhalifah (2016). To derive the sensitivity of the data to perturbations in the model parameters (The Born approximation), we define the perturbations $r_{v_{n1}^2}$, $r_{v_{n2}^2}$, $r_{v_v^2}$, r_{η_1}, r_{η_2} and r_{χ^2} as:

$$\begin{aligned} &v_{n1}^2 = v_{n1_0}^2(1+r_{v_{n1}^2}), v_{n2}^2 = v_{n2_0}^2(1+r_{v_{n2}^2}), v_v^2 = v_{v_0}^2(1+r_{v_v^2}),\\ &\eta_1 = \eta_{1_0}(1+r_{\eta_1}), \eta_2 = \eta_{2_0}(1+r_{\eta_1}), \chi^2 = \chi_0^2(1+r_{\chi^2}), \end{aligned} \tag{3}$$

where the subscript 0 denotes the background model parameters. To derive the radiation patterns for any parameterization, one can write the scattered field as follows (Masmoudi and Alkhalifah, 2016):

$$P_s = \omega^6 \int G_s(\mathbf{x_s},\mathbf{x},\omega)\mathbf{G_r}(\mathbf{x_r},\mathbf{x},\omega)\mathbf{a_i}(\mathbf{x})\cdot\mathbf{r_i}(\mathbf{x})\mathbf{dx}, \tag{4}$$

with r_i and a_i are the chosen parameters and their corresponding radiation patterns.

Our choice of parametrization is extracted from those suitable for reflection waveform inversion (RWI), described in Alkhalifah (2016) and Masmoudi and Alkhalifah (2017). In passive source inversion, the inversion for the unknown source images is similar to the inversion for the reflectivity in RWI. The estimation of the anisotropic parameters is obviously essential. In this abstract, we chose the parameterization $(v_{n_1}, \eta_1, \delta_1, \eta_d, \delta_d, \delta_3)$, where v_{n_1} is the normal moveout (NMO) velocity in $[x_2, x_3]$ plane, η_1, δ_1 are the anisotropic parameters defined in Tsvankin (1997) and Alkhalifah (2003) in $[x_2, x_3]$ plane, and η_d, δ_d are the deviation parameters defined in Masmoudi and Alkhalifah (2016), having the relations to Thomsen-Tsvankin parameters in the forms of:

$$\eta_d = \frac{\eta_2 - \eta_1}{1+2\eta_1}, \delta_d = \frac{\delta_2 - \delta_1}{1+2\delta_1}. \tag{5}$$

With the deviation parameters, an acoustic orthorhombic medium can be described by six parameters: three VTI parameters related to one vertical symmetry plane, two deviation parameters and one horizontal symmetry plane parameter Masmoudi and Alkhalifah (2016).

The radiation patterns for these parameters can be written as:

$$a(x) = \begin{pmatrix} 2 \\ 2sin^2\theta(1+cos^2\theta) \\ -2+2sin^2\theta \\ 2sin^2\theta sin^2\phi(cos^2\theta + 1 - sin^2\theta cos^2\phi) \\ 2sin^2\theta sin^2\phi(1 - sin^2\theta cos^2\phi) \\ 2sin^4\theta cos^2\phi sin^2\phi \end{pmatrix}, r(x) = \begin{pmatrix} r_{v_{n1}} \\ r_{\eta_1} \\ r_{\delta_1} \\ r_{\eta_d} \\ r_{\delta_d} \\ r_{\delta_3} \end{pmatrix}. \tag{6}$$

According to Figure 1, which shows the radiation patterns for this parameterization as a function of the scattering angle from a horizontal reflector for different azimuth angles, we may find that all three VTI parameters are azimuthally independent. v_{n_1} is independent of scattering angle as well, like in the isotropic case. η_1 is associated with large scattering angles, and δ_1 is mainly influenced by small scattering angles. The deviation parameters, η_d, δ_d, and the horizontal plane parameter δ_3 are azimuthally dependent. The η_d and δ_d affect the data mainly at larger azimuth angles and large scattering angles, which means there may be trade-offs between the two parameters. Moreover, note the weak scattering potential of δ_3. It indicates that δ_3 has little influence on the data recorded on the surface.

Considering observed data of the passive events on the Earth surface (or in a well), we can devise an iterative inversion by defining the optimization problem based on the classic least-square minimization of

$$E(m) = \frac{1}{2}\left\| d^{pred} - d^{obs} \right\|^2, \tag{7}$$

with respect to the source term and the model parameters, where d^{pred} is the predicted data generated from the current model, and d^{obs} is the observed data. We separate the source term into the dot product of a source image (indicating the source spatial information) and a source function (temporal information). Simultaneously, we invert for the source image, source function and model parameters. Due to the unknown source onset time, we are in danger of cycle skipping. To avoid this problem, we utilize a convolution objective function (Choi and Alkhalifah, 2011), which is reasonably source function independent. In this case, the objective function is given by:

$$E_{ind} = \sum_i^{nr} \|r_i\|^2 = \sum_i^{nr} \left\| d_i^{pred} * d_{ref}^{obs} - d_i^{obs} * d_{ref}^{pred} \right\|^2, \tag{8}$$

where d_i means the i^{th} trace both in the predicted and in the observed data and the d_{ref} means a reference trace. The reference trace is the same for observed and predicted data, and usually corresponding to the near offset trace per shot. The symbol $*$ is the convolution operator. In this new objective function, a predicted data source wavelet is convolved in both terms equally, which means the effect of the delay in the source wavelet $w(t)$ is muted. The gradient of the convolution objective function is calculated by taking the derivative of Equation 8 with respect to the model parameters, $m(x,z)$. The gradient can then be written as:

$$\frac{\partial E}{\partial m} = \sum_i^{nr} \left[\left(\frac{\partial d_i^{pred}}{\partial m} * d_{ref}^{obs} \right) \cdot r_i - \left(d_i^{obs} * \frac{\partial d_{ref}^{pred}}{\partial m} \right) \cdot r_i \right]. \tag{9}$$

Thus, the gradient involves calculating the adjoint wavefields with the adjoint sources:

$$\begin{aligned} R_i^{(1)} &= d_{ref}^{obs} \bigotimes \left(d_i^{pred} * d_{ref}^{obs} - d_i^{obs} * d_{ref}^{pred} \right), \\ R_i^{(2)} &= d_i^{obs} \bigotimes \left(d_i^{pred} * d_{ref}^{obs} - d_i^{obs} * d_{ref}^{pred} \right), \end{aligned} \tag{10}$$

at the i^{th} receiver position the reference trace position, respectively, where $\bigotimes$ is the cross-correlation operator. The two cross-correlated seismograms are back-propagated at the same time in order to reduce the computational cost (equivalent to FWI). More details about the source term separation and the convolved objective function can be found in our previous work Wang and Alkhalifah (2018).

Besides the adjoint sources, the gradients for each parameter of parameters $(v_{h_1}, \eta_1, \varepsilon_1, \eta_d, \varepsilon_d, \delta_3)$ have been given in a previous work by Masmoudi and Alkhalifah (2017). Simply using the chain rule the gradients for the new parameterization, we use here, can be derived which result in the gradients for the new parameterization given by combinations of $(v_{h_1}, \eta_1, \varepsilon_1, \eta_d, \varepsilon_d, \delta_3)$ gradients.

Considering the large number of parameters involved here and the potential for tradeoff, we use a multi-stage inversion strategy (Oh and Alkhalifah, 2016). In the first stage, an isotropic inversion can be applied to recover the NMO velocity. In the second stage, we focus on the VTI parameters, η_1 and δ_1. Finally, the three remaining parameters can be included into the inversion, along with the VTI parameters. The aim of this strategy is that the majority of the complexity of this nonlinear inversion is handled in the first stage, followed by inverting for the azimuthal independent VTI parameters. The inversion in each stage uses a nested approach, i.e. 1. inverting for the source images (spatial component); 2. inverting for the parameters for the stage; 3. updating the source function (temporal component). When updating the model parameters, a total variation regularization term is added in order to increase the robustness of the inversion.

NUMERICAL EXAMPLES

We present a synthetic test on a modified version of the SEG/EAGE orthorhombic overthrust model, shown in Figure 2. The model is $8km$ in the X, $6km$ in the Y and $4km$ in the Z directions. The model is discretized by a $25m$ grid interval in all three dimensions. For the observed data we considered 60 sources distributed in the blue box area shown in the v_{n_1} model in Figure 2, which is rather a small area reflecting a reservoir. The nature of the source distribution leads to limited illumination in the model, which is a challenge for any FWI. We record the data on the earth surface with every grid point at $Z = 0km$ plane acts as a receiver. We invert data filtered between $2Hz$ to $24Hz$ using the starting model parameters shown in Figure 3, which are strongly smoothed versions of the true ones. Note that δ_3 is set to zero in the initial model because it is quite difficult to estimate its value prior to the inversion.

We use the previously mentioned multi-stage model inversion strategy: updating first the isotropic model given by v_{n_1} (15 iterations) with a frequency band up to $8Hz$, then the VTI model by including η_1 and δ_1 with frequencies up to $16Hz$ (15 iterations), and finally the orthorhombic model by including η_d, δ_d and δ_3 with up to $24Hz$ data (15 iterations). We calculate the source image and the source function for each iteration with the model parameters for the current iteration. This inversion strategy takes advantage of the practical parameterization that allows for a continuity in the scattering potential of the model parameters as we move from higher symmetry anisotropy to lower ones. Figure 4 shows the final inverted results of all the parameters. Our inversion strategy shows a quite well recovered NMO velocity considering the limited illumination. The two thin reflectors in the upper part around $1km$ depth are accurately inverted. On the other hand, η_1 shows low resolution in the wave path part thanks to the transmission information and higher resolution on the sides in which eta can induce scattering. Although the resolution of η_1 is very limited, we still succeeded in inverting for the anticline structure above the sources, and the thin layer to the right of the anticline with low η_1 value. δ_1, which produces scattering mainly vertically as the radiation pattern suggests, shows low energy in the inverted results, which is a good match to the true model, because there is almost little structures in the true δ_1. η_d captures the azimuth variation in the velocity at large angles. Thus, the crossline component (in this case X) of the data shows details at the far angles, with little information in the Y direction, courtesy of the limited illumination provided by the sources. The inverted δ_d is also smooth and expected to experience some tradeoff with η_d, but seemingly its resolution is more focused on the deeper part again mostly in the X direction. δ_3 captures some information in both X and Y directions as it sensitivity is focused around the mid azimuth direction 45 degrees. On both left and right sides of the inveted results, some boundary artifacts can be found which is mainly caused by the illumination not covering those regions. In this case, of high number of parameters, we have no doubt that there are tradeoff in which we will explain in the presentation of the work in the meeting. Figures 5 to 7 show two sample shot gathers comparison between the initial, true and inverted ones, respectively. We note that the initial phases are cycle skipped from the true ones, while after the inversion, the early arrivals (transmissions) matches well to the true ones. As we mentioned above, in passive seismic we often rely on the transmission energy as scattering energy is weak. Nevertheless, we managed to also match some of the scattered energy, which probably yielded the higher resolution information. Figure 8 shows the convergence curve of the normalized data misfit function at different stages. After the 3 stages inversion, the total misfit reduces to 17%, which is a quite good value if we consider the poor illumination of the passive sources. The rapid decrease of the misfit in stages 1 and 2 show that the VTI parameters are better recovered. In stage 3, the curve does not decrease as much which indicates that the orthorhombic parameters have reduced influence on the data. In Figure 9, two sample inverted source images are shown. We may find most of the energy is well focused at the accurate locations (shown by the red lines), which means the model parameters are well recovered. There are some artifacts around the sources. The three-event nature of the source reflects the three early arrivals in our data, which indicates that some high-resolution information (reflectivity) in our model has leaked to our source image. We may further focus the energy by adding regularization terms or using other norm objective functions, such as L1-norm.

CONCLUSIONS

We developed an approach to invert for the source spatial image, the source temporal wavelet and the anisotropic model parameters that describe an orthrohombic anisotropic acoustic medium using recorded passive seismic data. To mitigate the role of the source wavelet, which is usually inaccurate in shape or time due to inaccuracies in model parameters, we utilize an alternative objective function based on the convolution of our recorded traces with a reference trace. A multistage inversion for the anisotropic parameters, with the proper parametrization, yielded convergent results for the modified 3D orthorhombic SEG/EAGE model, in spite of starting with crude initial conditions.

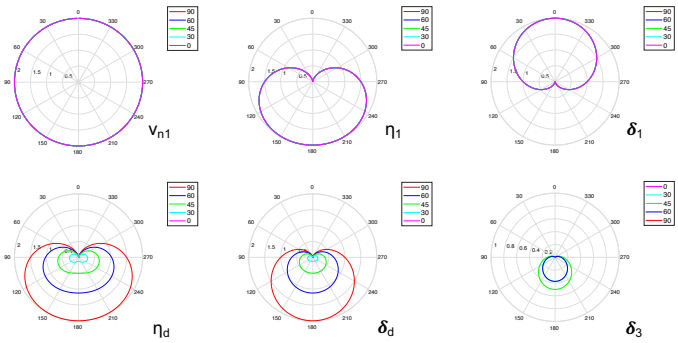

Figure 1: Radiation patterns corresponding to scattering from a horizontal reflector of perturbations in the parameters with $(v_{n_1}, \eta_1, \delta_1, \eta_d, \delta_d, \delta_3)$. The radial direction reflects the scattering potential, while the polar angle corresponds to the scattering angle. The azimuth is given by the colors.

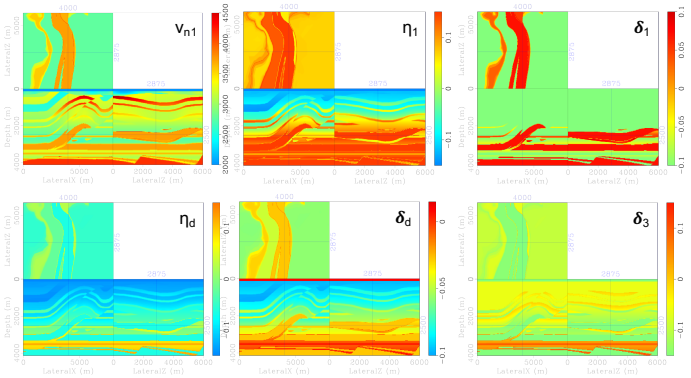

Figure 2: The true model parameters. 60 shots are generated inside the blue box showed in v_{n_1}.

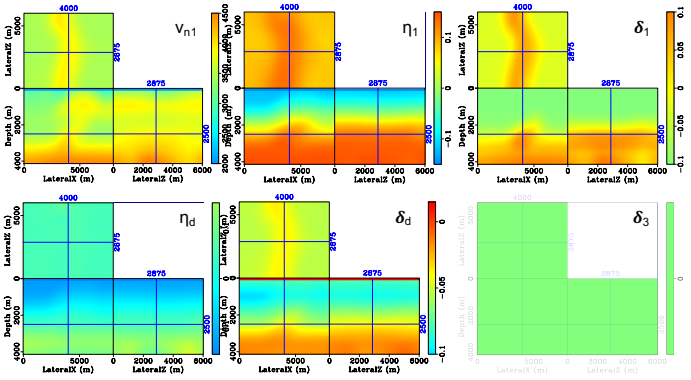

Figure 3: The initial model parameters, generated by strongly smoothing the true parameters.

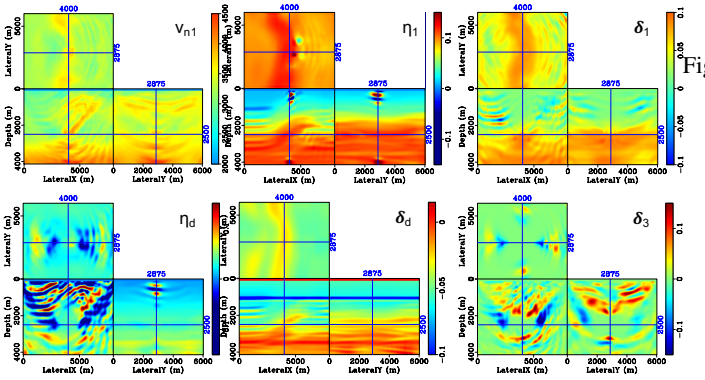

Figure 4: The inverted model parameters after multi stages inversion strategy.

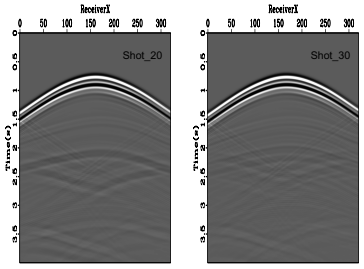

Figure 5: The initial shot gathers of shot No. 20 & 30.

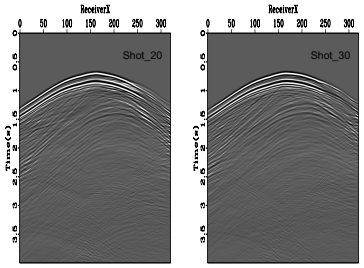

Figure 6: The true shot gathers of shot No. 20 & 30.

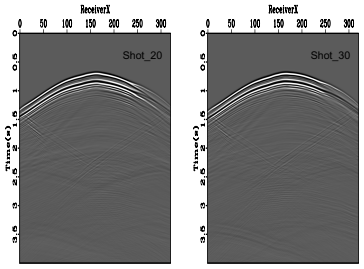

Figure 7: The inverted shot gathers of shot No. 20 & 30.

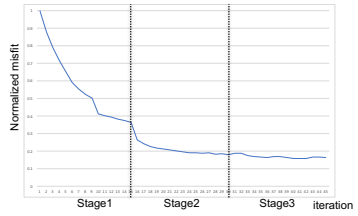

Figure 8: Normalized objective convergence curve.

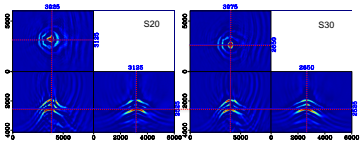

Figure 9: The inverted source images for the sample sources No.20 & 30.

ACKNOWLEDGMENT

We thank KASUT and KAUST Supercomputing Lab for supporting to this research. We thank SWAG members for their helpful discussion. We specially thank Dr. Nabil Masmoudi for his help in the orthorhombic inversion and the codes.

REFERENCES

Alkhalifah, T., 2003, An acoustic wave equation for orthorhombic anisotropy: Geophysics, **68**, 1169–1172.

———, 2016, Research note: Insights into the data dependency on anisotropy: An inversion prospective: Geophysical Prospecting, **64**, 505–513.

Choi, Y., and T. Alkhalifah, 2011, Source-independent time-domain waveform inversion using convolved wavefields: Application to the encoded multisource waveform inversion: Geophysics, **76**, R125–R134.

Eisner, L., P. M. Duncan, W. M. Heigl, and W. R. Keller, 2009, Uncertainties in passive seismic monitoring: The Leading Edge, **28**, 648–655.

Grechka, V., and S. Yaskevich, 2013, Azimuthal anisotropy in microseismic monitoring: A bakken case study: Geophysics, **79**, KS1–KS12.

Ibanez-Jacome, W., T. Alkhalifah, and U. b. Waheed, 2014, Effective orthorhombic anisotropic models for wavefield extrapolation: Geophysical Journal International, **198**, 1653–1661.

Kaderli, J., M. D. McChesney, S. E. Minkoff, et al., 2015, Microseismic event estimation in noisy data via full waveform inversion: Presented at the 2015 SEG Annual Meeting, Society of Exploration Geophysicists.

Masmoudi, N., and T. Alkhalifah, 2016, A new parameterization for waveform inversion in acoustic orthorhombic mediaorthorhombic parameterization: Geophysics, **81**, R157–R171.

———, 2017, Waveform inversion in acoustic orthorhombic media with a practical set of parameters, *in* SEG Technical Program Expanded Abstracts 2017: Society of Exploration Geophysicists, 1659–1665.

Nakata, N., and G. C. Beroza, 2016, Reverse time migration for microseismic sources using the geometric mean as an imaging condition: Geophysics, **81**, KS51–KS60.

Oh, J.-W., and T. Alkhalifah, 2016, Elastic orthorhombic anisotropic parameter inversion: An analysis of parameterizationelastic orthorhombic anisotropic fwi: Geophysics, **81**, C279–C293.

Sun, J., Z. Xue, T. Zhu, S. Fomel, and N. Nakata, 2016, Full-waveform inversion of passive seismic data for sources and velocities, *in* SEG Technical Program Expanded Abstracts 2016: Society of Exploration Geophysicists, 1405–1410.

Tsvankin, I., 1997, Anisotropic parameters and p-wave velocity for orthorhombic media: Geophysics, **62**, 1292–1309.

Van Der Baan, M., D. Eaton, M. Dusseault, et al., 2013, Microseismic monitoring developments in hydraulic fracture stimulation: Presented at the ISRM International Conference for Effective and Sustainable Hydraulic Fracturing, International Society for Rock Mechanics and Rock Engineering.

Wang, H., and T. Alkhalifah, 2017, Time reversal migration for passive sources using a maximum variance imaging condition: Presented at the 79th EAGE Conference and Exhibition 2017.

———, 2018, Microseismic imaging using a source function independent full waveform inversion method: Geophysical Journal International, **214**, 46–57.

Warpinski, N., et al., 2009, Microseismic monitoring: Inside and out: Journal of Petroleum Technology, **61**, 80–85.